



# First principles studies of superhard BC<sub>6</sub>N phases with unexpected 1D metallicity

Yufei Gao<sup>a</sup>, Yingju Wu<sup>a</sup>, Quan Huang<sup>b</sup>, Mengdong Ma<sup>a</sup>, Yilong Pan<sup>a</sup>, Mei Xiong<sup>a</sup>, Ziheli Li<sup>a</sup>, Zhisheng Zhao<sup>a</sup>, Julong He<sup>a</sup>, Dongli Yu<sup>a,\*</sup>

<sup>a</sup>State Key Laboratory of Metastable Materials Science and Technology, Yanshan University, Qinhuangdao 066004, Hebei Province, China

<sup>b</sup>Center for High Pressure Science & Technology Advanced Research 1690 Cailun Rd, Bldg. #6, Pudong, Shanghai 201203, China

HPSTAR  
608-2018

## ARTICLE INFO

### Article history:

Received 14 November 2017

Received in revised form 30 January 2018

Accepted 5 February 2018

Available online 24 February 2018

### Keywords:

BC<sub>6</sub>N

First principles calculations

Metallicity

Superhard

## ABSTRACT

Three novel  $sp^2$ - $sp^3$  hybridized BC<sub>6</sub>N phases with a sandwich structure, including a type of orthorhombic BC<sub>6</sub>N (*o*-BC<sub>6</sub>N) and two types of tetragonal BC<sub>6</sub>N (*t*-BC<sub>6</sub>N-1 and *t*-BC<sub>6</sub>N-2), are investigated through first principles calculations. The structural stabilities are confirmed by the calculated elastic constants and phonon dispersions. Calculated electronic band structures, density of states (DOS), and partial DOS show that the *o*-BC<sub>6</sub>N, *t*-BC<sub>6</sub>N-1, and *t*-BC<sub>6</sub>N-2 crystals may possess the metallicity with the conducting electrons from the *p* orbitals of  $sp^2$ -hybridized C atoms. Calculations of electron orbits indicate that the electrons in *o*-BC<sub>6</sub>N and *t*-BC<sub>6</sub>N-1 structures can conduct through the  $\pi$  bonds along the orientation parallel to the [1 0 0] and [0 1 0] directions in different layers. Moreover, the electrons in *t*-BC<sub>6</sub>N-2 structure can conduct along the orientation parallel to the [1 1 0] and  $[\bar{1}$  1 0] directions in different layers. The behavior of the linear electron conductivity in the layer and vertical direction of conduction between the adjacent layers imply that the three kinds of crystals have potential applications in the field-effect devices. Calculation results using the semi-empirical microscopic model show that *o*-BC<sub>6</sub>N, *t*-BC<sub>6</sub>N-1, and *t*-BC<sub>6</sub>N-2 are potential superhard materials with Vickers hardness of 52.4, 45.3, and 40.1 GPa, respectively.

© 2018 Elsevier B.V. All rights reserved.

## 1. Introduction

Diamond and cubic boron nitrogen (*c*-BN) are the hardest solids that have some kinds of significant properties, such as extreme hardness, high thermal conductivity, large elastic constants, bulk modulus, wide band gaps, and superior melting temperatures [1–4]. However, diamond can react with ferrous alloys easily and oxidizes at approximate 600 °C in air [5]. Although *c*-BN is more chemically inactive and has a high oxidation resistant temperature (~1100 °C) [6], it is only half as hard as diamond. Thus, searching for potential superhard crystals is meaningful to compensate for the weakness between diamond and *c*-BN. Ternary boron-carbon-nitrogen (B-C-N) compounds as potential candidates have received considerable attention in experimental [7–10] and theoretical [11–14] studies. Basing on the diamond structure, researchers have replaced C atoms with B and N atoms to obtain zinc-blende-structure ternary B-C-N phases. Particularly, diamond-like cubic BC<sub>2</sub>N (*c*-BC<sub>2</sub>N) phase, which are regarded as an ideal mixture of diamond and *c*-BN, has been investigated extensively [7,9,11,15–17].

Graphite-like BC<sub>6</sub>N (*g*-BC<sub>6</sub>N) [9] was synthesized using chemical vapor deposition at 1500–1800 °C. Seebeck coefficient test suggested that *g*-BC<sub>6</sub>N is an n-type semiconductor, which was demonstrated by the consequence of soft X-ray emission spectra. Strictly speaking, cubic BC<sub>6</sub>N (*c*-BC<sub>6</sub>N) has not been compounded to date. Andrzej R. Badzian [18] obtained solid solutions of the sphalerite structural diamond and *c*-BN with the composition of (BN)<sub>0.26</sub>C<sub>0.74</sub> under high pressure and high temperature. The stoichiometric atomic ratio of the high dense (BN)<sub>0.26</sub>C<sub>0.74</sub> crystal is highly approximate to that of BC<sub>6</sub>N. Luo et al. [13] constructed two possible metastable high density BC<sub>6</sub>N phases originating from the diamond structure. According to their reports, the Vickers hardness of two BC<sub>6</sub>N phases is about 79–80 GPa. These values are higher than that of the *c*-BC<sub>2</sub>N [7] phases (76 GPa) but still lower than that of diamond. The calculated electronic band structures have proved that two BC<sub>6</sub>N phases are both direct band gap semiconductors. Most of the formula BC<sub>*x*</sub>N (*x* = 2, 4, 6) compounds are either insulators or semiconductors in which (BN) and C<sub>*x*</sub> units are isoelectronic. Ternary B-C-N solids would become conductors when the quantity of B atoms is not equal to that of N atoms because B, C, and N atoms possess different valence electrons

\* Corresponding author.

E-mail address: [ydl@ysu.edu.cn](mailto:ydl@ysu.edu.cn) (D. Yu).

(3, 4, and 5, respectively). A  $P$ -42  $m$  structural electron-deficient metallic tetragonal ( $t$ - $B_2CN$ ) was studied theoretically [19].

Li et al. [20] recently discovered a novel hexagonal  $B_3N_5$  ( $h$ - $B_3N_5$ ) structure constructed from the planar hexagonal BN layers sandwiched with  $N_2$  molecules by using the particle swarm optimization technique. First-principle calculations indicated that  $h$ - $B_3N_5$  can transform into ambient metastable orthorhombic  $C22_1$ - $B_3N_5$  phase under high pressure.  $C22_1$ - $B_3N_5$  is a high energy density structure with a narrow band gap of 0.775 eV. The Vickers hardness of  $C22_1$ - $B_3N_5$  is about 44 GPa, making it a superhard material. In the previous work, we have reported a novel  $sp^2$ - $sp^3$  mixed hybridized  $o$ - $BC_2N$  [21] structure, which possesses fascinating electronic property of the linear-planar metallicity with Vickers hardness about 41.2 GPa, by replacing parts of the B and N atoms with C atoms in the  $C22_1$ - $B_3N_5$  unit cell.

In this paper, we report three possible  $BC_6N$  phases, including  $o$ - $BC_6N$ ,  $t$ - $BC_6N$ -1, and  $t$ - $BC_6N$ -2, by replacing parts of the B and N atoms with C atoms in the  $C22_1$ - $B_3N_5$  phase. The mechanical and electrical properties of the three crystals were predicted using first-principle calculations.

## 2. Calculation methods

By replacing part of B and N atoms with C atoms in the  $o$ - $B_3N_5$  unit cell, three  $BC_6N$  crystals with sandwich-like structure are constructed from multi-layers of C atoms sandwiched between the layers of B and N atoms along the  $c$  axis. In these structures, the  $sp^3$ -hybridized B, C, and N atoms and  $sp^2$ -hybridized C atoms coexist. After the structural parameters were geometry optimized, bulk modulus, shear modulus, total energies, and formation energies were calculated in detail using the pseudopotential density functional method [22] implemented in the CASTEP code [23–26].

The Perdew-Berke-Ernzerhof form of the generalized gradient approximation was used to treat the exchange-correlation function [27]. The norm-conserving pseudopotential [28] with energy of cutoff was 770 eV. The  $k$ -points were selected with  $7 \times 7 \times 4$  in

the Brillouin zone at the mesh space according to the Monkhorst-Pack scheme [29]. Using the CASTEP code, elastic constants, bulk modulus, and shear modulus can be calculated directly. Electron-phonon coupling and phonon dispersion curves were studied within the frame of plane-wave pseudopotential method and density functional perturbation theory [30] implemented in the Quantum ESPRESSO package. The structural relaxation was processed by the Broyden-Fletcher-Goldfarb-Shanno (BFGS) methods [31]. On the basis of our microscopic theoretical model [32–35] for covalent dominant crystals, the Vickers hardness can be calculated by the following formula:  $H_v$  (GPa) =  $AN_e^{2/3}d^{-2.5}\exp^{-1.191f_i-32.2f_m^{0.55}}$ , where  $A$  is a constant as 350,  $N_e$  is the electron density,  $d$  is the average bond length,  $f_i$  is the Phillips ionicity of the chemical bond, and  $f_m$  is a factor of metallicity.  $f_i$  can be calculated by the equation:  $f_i = [1 - \exp(-|P_c - P|/P)]^{0.735}$  [33];  $f_m$  can be written as  $f_m = 0.026D_F/n_e$  [34], where  $D_F$  is the electron density of states at the Fermi level and  $n_e$  is the total number of the valence electrons in a unit cell.

## 3. Results and discussions

After structural relaxation, the crystal structures of  $o$ - $BC_6N$ ,  $t$ - $BC_6N$ -1, and  $t$ - $BC_6N$ -2 are displayed in Fig. 1. Their corresponding atomic Wyckoff positions are listed in Table 1. The  $o$ - $BC_6N$  and  $t$ - $BC_6N$ -1 form sandwich-like layered structures, with one layer of B and N and multi-layers of C atoms along the  $c$  axis. The  $t$ - $BC_6N$ -2 is constructed from the interlinked multi-layers of C sandwiched between blocks of  $B_2CN_2$  along the  $c$  axis. The  $B_2CN_2$  block is composed of two BN sheets and one carbon sheet. Three  $BC_6N$  structures contain  $sp^2$ -hybridized C–C bonds and  $sp^3$ -hybridized C–C, C–B, and C–N bonds.  $Sp^3$ -hybridized B–N bonds present in  $o$ - $BC_6N$  and  $t$ - $BC_6N$ -1 and they are not found in  $t$ - $BC_6N$ -2 structure.

The lattice parameters, total energies  $E_t$ , formation energies  $E_f$ , and bulk modulus  $B$  of the three  $BC_6N$  structures are listed in Table 2. We calculated the lattice parameters of diamond and

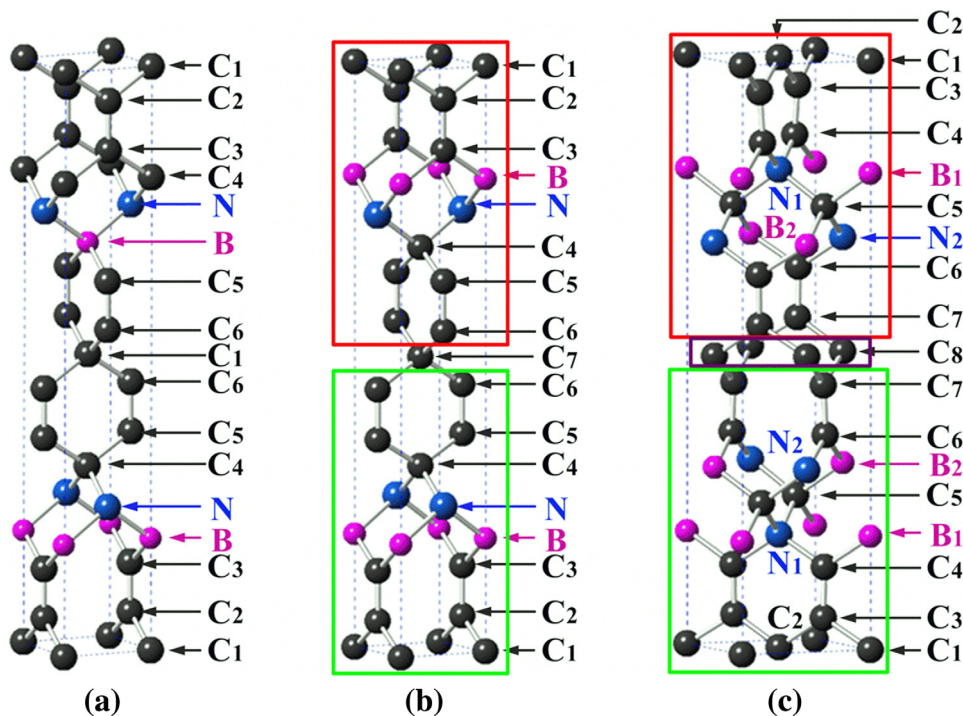


Fig. 1. The relaxed crystal structures of  $o$ - $BC_6N$  (a),  $t$ - $BC_6N$ -1(b), and  $t$ - $BC_6N$ -1(c). The boron, carbon, and nitrogen atoms are described as pink, black, and blue colors, respectively. (For interpretation of the references to color in this figure legend, the reader is referred to the web version of this article.)

**Table 1**  
Atomic Wyckoff positions of the *o*-BC<sub>6</sub>N, *t*-BC<sub>6</sub>N-1, and *t*-BC<sub>6</sub>N-2 structures.

<i>o</i> -BC <sub>6</sub> N		<i>t</i> -BC <sub>6</sub> N-1		<i>t</i> -BC <sub>6</sub> N-2	
Atom	Wyckoff positions	Atom	Wyckoff positions	Atom	Wyckoff positions
B	2a (0.5, 0.5, 0.691)	B	2e (0, 0, 0.807)	B <sub>1</sub>	2g (-0.5, 0, -0.308)
N	2b (0, 0.5, 0.252)	N	2g (0, 0.5, 0.254)	B <sub>2</sub>	2e (0, 0, -0.808)
C <sub>1</sub>	2b (0.5, 0, 0.051)	C <sub>1</sub>	1a (0, 0, 0)	N <sub>1</sub>	2g (-0.5, 0.5, -0.690)
C <sub>2</sub>	2b (0.5, 0, 0.137)	C <sub>2</sub>	2g (0.5, 0, 0.052)	N <sub>2</sub>	2f (-0.5, -0.5, -0.809)
C <sub>3</sub>	2a (0.5, 0.5, 0.311)	C <sub>3</sub>	2g (0.5, 0, 0.139)	C <sub>1</sub>	1a (0, 0, 0)
C <sub>4</sub>	2a (0.5, 0.5, 0.498)	C <sub>4</sub>	2f (0.5, 0.5, 0.313)	C <sub>2</sub>	1c (-0.5, -0.5, 0)
C <sub>5</sub>	2b (0.5, 0, 0.861)	C <sub>5</sub>	1c (0.5, 0.5, 0.5)	C <sub>3</sub>	4h (-0.248, -0.262, -0.052)
C <sub>6</sub>	2b (0.5, 0, 0.946)	C <sub>6</sub>	2g (0, 0.5, 0.551)	C <sub>4</sub>	4h (-0.266, -0.244, -0.138)
		C <sub>7</sub>	2g (0, 0.5, 0.637)	C <sub>5</sub>	4h (-0.249, 0.225, -0.250)
				C <sub>6</sub>	2g (-0.5, 0, -0.497)
				C <sub>7</sub>	4h (-0.259, 0.244, -0.552)
				C <sub>8</sub>	4h (-0.248, -0.234, -0.638)

**Table 2**  
Lattice parameters, total energy ( $E_t$ ), formation energy ( $E_f$ ), bulk modulus  $B$ , and elastic stiffness constants of the *o*-BC<sub>6</sub>N, *t*-BC<sub>6</sub>N-1, and *t*-BC<sub>6</sub>N-2 structures after structural optimization. As a comparison, the corresponding values for BC<sub>6</sub>N-1 and *r*-BC<sub>6</sub>N are also listed.

Structure Symmetry	<i>o</i> -BC <sub>6</sub> N-1 Im $m$ 2	<i>t</i> -BC <sub>6</sub> N-1 $P$ -4 $m$ 2	<i>t</i> -BC <sub>6</sub> N-2 $P$ -4	BC <sub>6</sub> N-1 <sup>a</sup> $P$ -42 $M$	<i>r</i> -BC <sub>6</sub> N <sup>b</sup> R3 $M$
$a$ (Å)	2.628	2.587	3.692	3.560	3.565
$b$ (Å)	2.569	2.587	3.692	3.572	3.565
$c$ (Å)	15.804	15.784	15.654	3.572	3.565
$\alpha$ $\beta$ $\gamma$ (deg)	90	90	90	90	90.15
$E_t$ (eV/atom)	-159.09	-159.44	-159.27	-160.04	-160.58
$E_f$ (eV/atom)	0.946	0.591	0.766	0.441	0.331
$B$ (GPa)	313.4	317.8	293.3	412.7	399.9
$G$ (GPa)	177.6	149.1	183.3		
$c_{11}$	724.7	645.9	464.9		977.0
$c_{22}$	661.8				
$c_{33}$	986.2	1001.5	957.1		986.1
$c_{44}$	81.4	68.16	122.5	525.4	529.1
$c_{55}$	130.9				
$c_{66}$	121.4	123.8	291.9		433.6
$c_{12}$	37.7	96.0	235.5		109.8
$c_{13}$	75.9	108.4	83.1		109.8
$c_{23}$	139.6				

<sup>a</sup> Ref. [38].

<sup>b</sup> Ref. [13].

*c*-BN of 3.568 and 3.627 Å, respectively, which are close to the experimental values of 3.567 Å for diamond and 3.615 Å for *c*-BN [8]. These results indicate that the calculated results are satisfactory. For *o*-BC<sub>6</sub>N, the lattice constants  $a$ ,  $b$ , and  $c$  are 2.628, 2.569, and 15.804 Å, respectively. For *t*-BC<sub>6</sub>N-1, the relaxed structural parameter is  $a = b = 2.587$  Å; this value is between the lattice parameter  $a$  and  $b$  of the *o*-BC<sub>6</sub>N phase. For *t*-BC<sub>6</sub>N-2, the relaxed structural parameter is  $a = b = 3.629$  Å, which is much bigger than the lattice parameters  $a$  or  $b$  of the *o*-BC<sub>6</sub>N and *t*-BC<sub>6</sub>N-1 phases. The lattice constants  $c$  of *t*-BC<sub>6</sub>N-1 and *t*-BC<sub>6</sub>N-2 are 15.784 and 15.654 Å, which are much closer to the lattice  $c$  of the *o*-BC<sub>6</sub>N phase. The *t*-BC<sub>6</sub>N-1 structure has the lowest total energy ( $E_t$ ) than the two other BC<sub>6</sub>N structures. This result is consistent with the bond counting rule [36,37]. The formation energy ( $E_f$ ) of the BC<sub>6</sub>N phase is calculated using the following formula:  $E_f = E_{BC_6N} - (E_{c-BN} + 6E_C)$ , where  $E_{BC_6N}$ ,  $E_{c-BN}$ , and  $E_C$  represent the energy of BC<sub>6</sub>N, *c*-BN, and diamond formula unit, respectively. All the phases have positive formation energies, this result indicates that these BC<sub>6</sub>N phases are metastable and tend to separate into *c*-BN and diamond, which is similar to the BC<sub>2</sub>N [11] and BC<sub>6</sub>N [13]. The calculated bulk modulus  $B$  of *o*-BC<sub>6</sub>N, *t*-BC<sub>6</sub>N-1, and *t*-BC<sub>6</sub>N-2 are 313.4, 317.8, and 293.3 GPa, respectively. These values are smaller than that of diamond (443 GPa) and *c*-BN (400 GPa) [22].

To check the mechanical stabilities of the BC<sub>6</sub>N crystals, we calculated their elastic stiffness constants. For the orthorhombic structures, the generalized elastic stability criteria are  $C_{11} > 0$ ,

$C_{22} > 0$ ,  $C_{33} > 0$ ,  $C_{44} > 0$ ,  $C_{55} > 0$ ,  $C_{66} > 0$ ,  $[C_{11} + C_{22} + C_{33} + 2(C_{12} + C_{13} + C_{23})] > 0$ ,  $(C_{11} + C_{22} - 2C_{12}) > 0$ ,  $(C_{11} + C_{33} - 2C_{13}) > 0$ , and  $(C_{22} + C_{33} - 2C_{23}) > 0$  [39]. For the tetragonal structures, the restrictions are  $C_{ii} > 0$  ( $i = 1, 3, 4, 6$ ),  $(C_{11} - C_{12}) > 0$ ,  $(C_{11} + C_{33} - 2C_{13}) > 0$ , and  $[2(C_{11} + C_{12}) + C_{33} + 4C_{13}] > 0$  [39]. The elastic stiffness constant  $c_{ij}$  values are listed in Table 2. The results showed that all three BC<sub>6</sub>N crystals satisfy the corresponding restrictions mentioned above, suggesting that they are mechanically stable. To explore the dynamical stability, we calculated the phonon dispersion curves of *o*-BC<sub>6</sub>N, *t*-BC<sub>6</sub>N-1, and *t*-BC<sub>6</sub>N-2, respectively. The computed results are shown in Fig. 2. At ambient conditions, three structures are dynamically stable because of the absence of the imaginary frequencies in the whole Brillouin zone.

The electronic band structures at the equilibrium geometries were studied, and the results are presented in Fig. 3. The calculated results in the *o*-BC<sub>6</sub>N structure show the presence of three occupied bands crossing the Fermi level (the red bands in Fig. 3a); this result suggests that the *o*-BC<sub>6</sub>N phase may display metallicity property. Similarly, several occupied bands cross the Fermi level (the red bands in Fig. 3b and c, respectively) in *t*-BC<sub>6</sub>N-1 and *t*-BC<sub>6</sub>N-2. These results indicate that the *t*-BC<sub>6</sub>N-1 and *t*-BC<sub>6</sub>N-2 crystals may also possess the property of metallicity. To identify which atoms would contribute at the Fermi level and bring about the structural conductivity, we calculated the total density of states (DOS) and partial density of states (PDOS) for B, C, and N atoms in the unit cell of *o*-BC<sub>6</sub>N, *t*-BC<sub>6</sub>N-1 and *t*-BC<sub>6</sub>N-2,

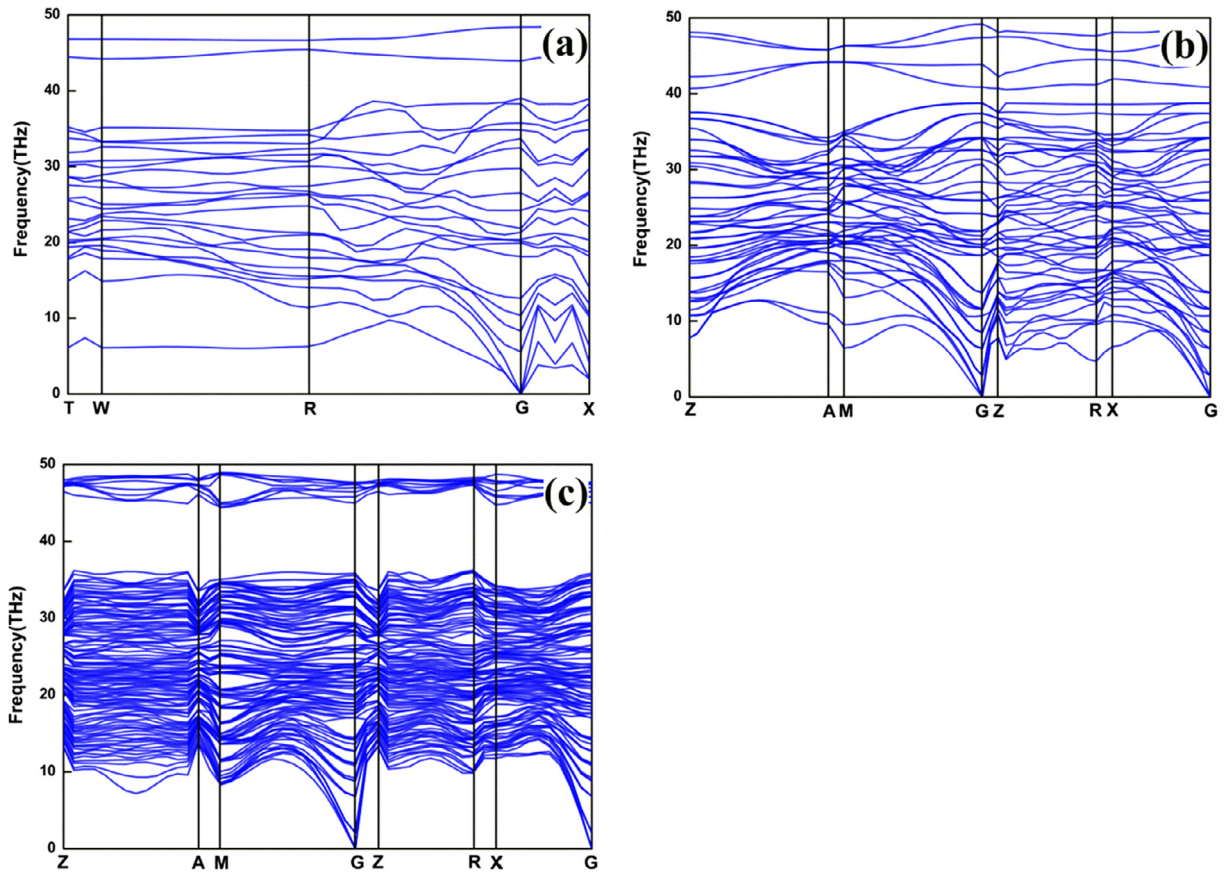


Fig. 2. The phonon dispersion curves for *o*-BC<sub>6</sub>N (a), *t*-BC<sub>6</sub>N-1 (b), and *t*-BC<sub>6</sub>N-2 (c).

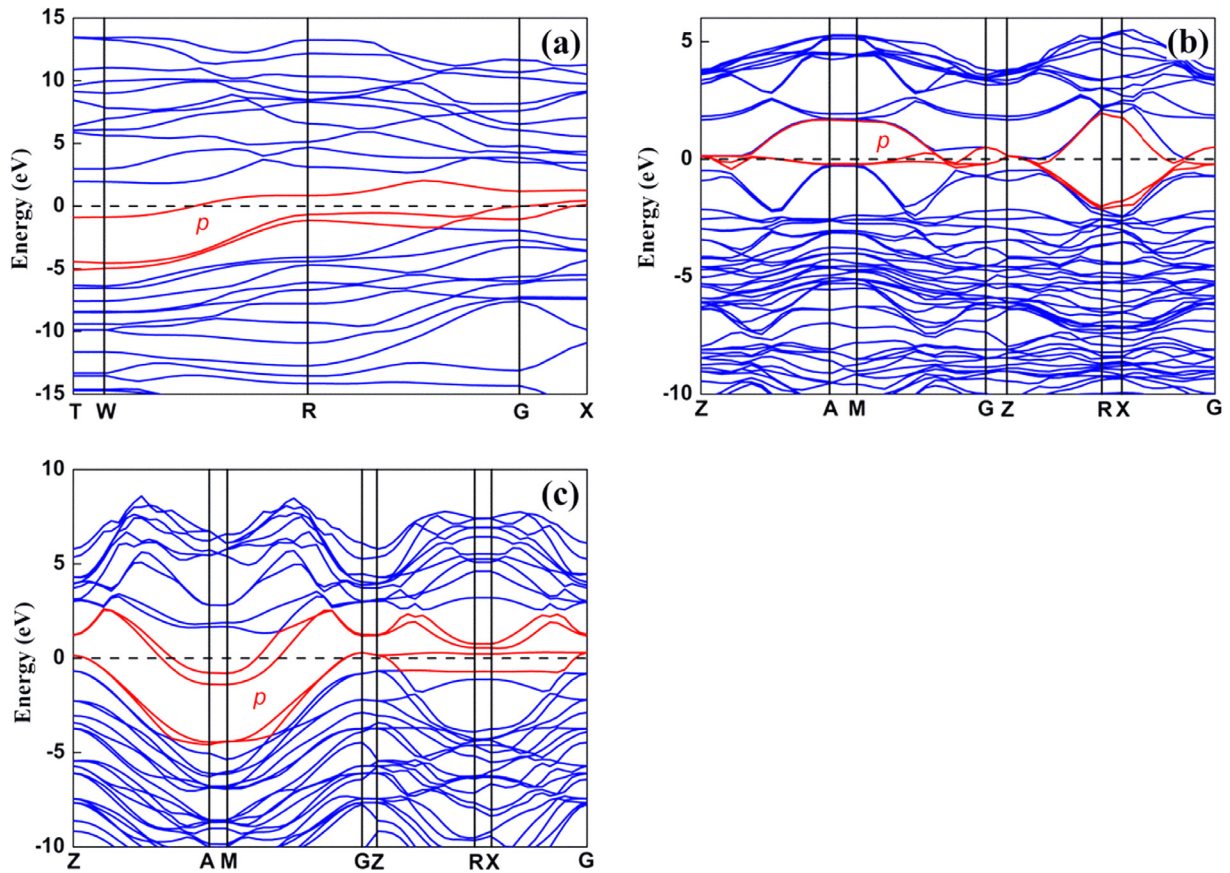
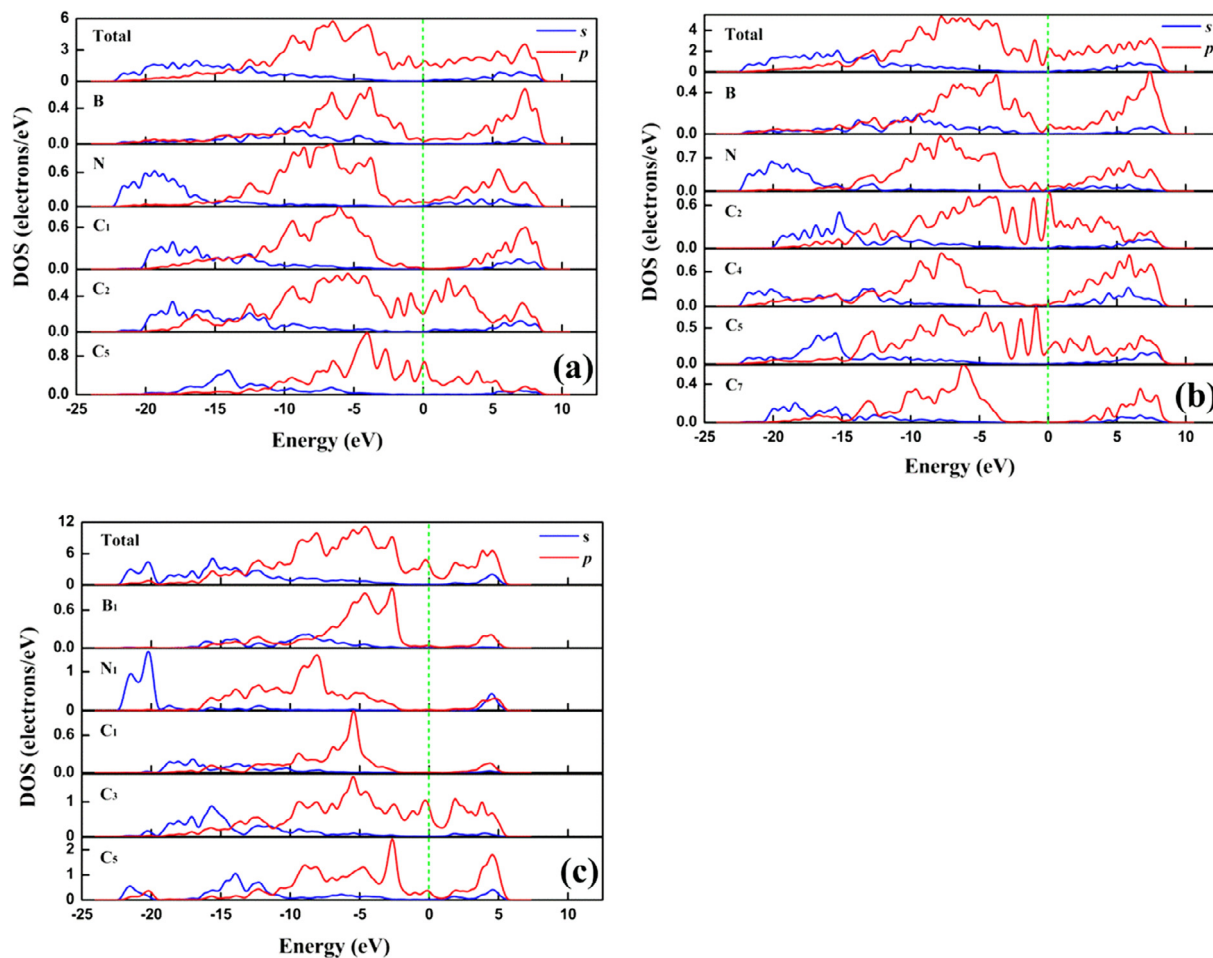


Fig. 3. The electronic structures of *o*-BC<sub>6</sub>N (a), *t*-BC<sub>6</sub>N-1 (b), and *t*-BC<sub>6</sub>N-2 (c). The Fermi level is indicated by the horizontal dashed line.



**Fig. 4.** Total density of states, *s* (blue line) and *p* (red line) partial density of states of the *o*-BC<sub>6</sub>N (a), *t*-BC<sub>6</sub>N-1 (b), and *t*-BC<sub>6</sub>N-2 (c) structures. The Fermi level is indicated by green dashed line. (For interpretation of the references to color in this figure legend, the reader is referred to the web version of this article.)

respectively. The calculated DOS and PDOS of the B, N and C<sub>*i*</sub> (*i* = 1 ~ 6) atoms in the *o*-BC<sub>6</sub>N structure are shown in Fig. 4a. At the Fermi level, the conducting electrons were mostly from the *p* electrons of *sp*<sup>2</sup>-hybridized C<sub>2</sub>, C<sub>3</sub>, C<sub>5</sub>, and C<sub>6</sub> atoms. The calculated total DOS and the PDOS of the B, N, and C<sub>*j*</sub> (*j* = 1 ~ 7) atoms in the *t*-BC<sub>6</sub>N-1 structure are shown in Fig. 4b. The conducting electrons at the Fermi level were mostly from the *p* electrons of *sp*<sup>2</sup>-hybridized C<sub>2</sub>, C<sub>3</sub>, C<sub>5</sub>, and C<sub>6</sub> atoms. The calculated DOS and PDOS of the B<sub>1</sub>, N<sub>1</sub>, and C<sub>*k*</sub> (*k* = 1 ~ 8) atoms in the *t*-BC<sub>6</sub>N-2 structure are shown in Fig. 4c. The conducting electrons at the Fermi level were mostly from the *p* electrons of *sp*<sup>2</sup>-hybridized C<sub>3</sub>, C<sub>4</sub>, C<sub>6</sub>, and C<sub>7</sub> atoms. Consequently, the metallicity of three BC<sub>6</sub>N came from the *sp*<sup>2</sup>-hybridized C atoms. The *sp*<sup>3</sup>-hybridized atoms play a major role in blocking electronic conduction.

In the *t*-BC<sub>6</sub>N-1 structure, if the partial structure (the green square in Fig. 1b) below C<sub>7</sub> atom is rotated 90 degree around the *c* axis, the two parts of constitution (the red and green squares in Fig. 1b) above and below the C<sub>7</sub> atomic layer will become mirror symmetry. We can also obtain a mirror symmetry structure in the *t*-BC<sub>6</sub>N-2 structures by spinning the partial structures below the C<sub>8</sub> layer in *t*-BC<sub>6</sub>N-2 to 90 degree around the *c* axis. This dramatic structural symmetry may lead to the orthogonal conduction electron migration ways in above the BC<sub>6</sub>N structures. To understand the directional movements of the excited electrons in the *o*-BC<sub>6</sub>N structure under varying electric fields, we calculated the electron orbits around the Fermi level (red bands in Fig. 3) as shown in Fig. 5.

In Fig. 5a and b, the possible conduction electron orbits in the *o*-BC<sub>6</sub>N partially overlap on the [1 0 0] and [0 1 0] crystal orientations along the C<sub>2</sub>–C<sub>3</sub> (A region) and C<sub>5</sub>–C<sub>6</sub> (B region) diatomic chains, respectively. In the C and D regions, the overlap of the electron orbits enveloping the C<sub>5</sub>–C<sub>6</sub> and C<sub>2</sub>–C<sub>3</sub> diatomic units shows an orthogonal relationship with that in the B and A regions. These overlapped electric orbits are disconnected in the [0 0 1] crystal orientation. The distribution of the electron orbits around the Fermi level indicates that a novel layer one-dimensional (1D) electric conductivity with orthogonal relationship between the neighboring layers is present in the *o*-BC<sub>6</sub>N crystal.

Based on the same method, we also found the 1D metallicity with the orthogonal directionality between the alternant atomic layers in the *t*-BC<sub>6</sub>N-1 and *t*-BC<sub>6</sub>N-2 structures shown as in Fig. 5 (c)–(f). In the *t*-BC<sub>6</sub>N structures, this orthogonal 1D conductivity is consistent with their unique crystal symmetry. If the crystal with the orthogonal distribution of 1D electric conductivity is placed in a changing magnetic or electric field, we will find that their 1D conductivity will change regularly with the direction or intensity of the field. Thus, this phenomenon implies that the single crystals of *o*-BC<sub>6</sub>N, *t*-BC<sub>6</sub>N-1, and *t*-BC<sub>6</sub>N-2 may be suitable candidate materials to be used as probe in the field strength or direction measuring. In addition, considering the metallicity of the three proposed BC<sub>6</sub>N structures, using our hardness model, and considering the metallicity of the three proposed BC<sub>6</sub>N structures, we estimated the Vickers hardness values of *o*-BC<sub>6</sub>N, *t*-BC<sub>6</sub>N-1, and *t*-BC<sub>6</sub>N-2. Their bond parameters obtained from first-principle calculations

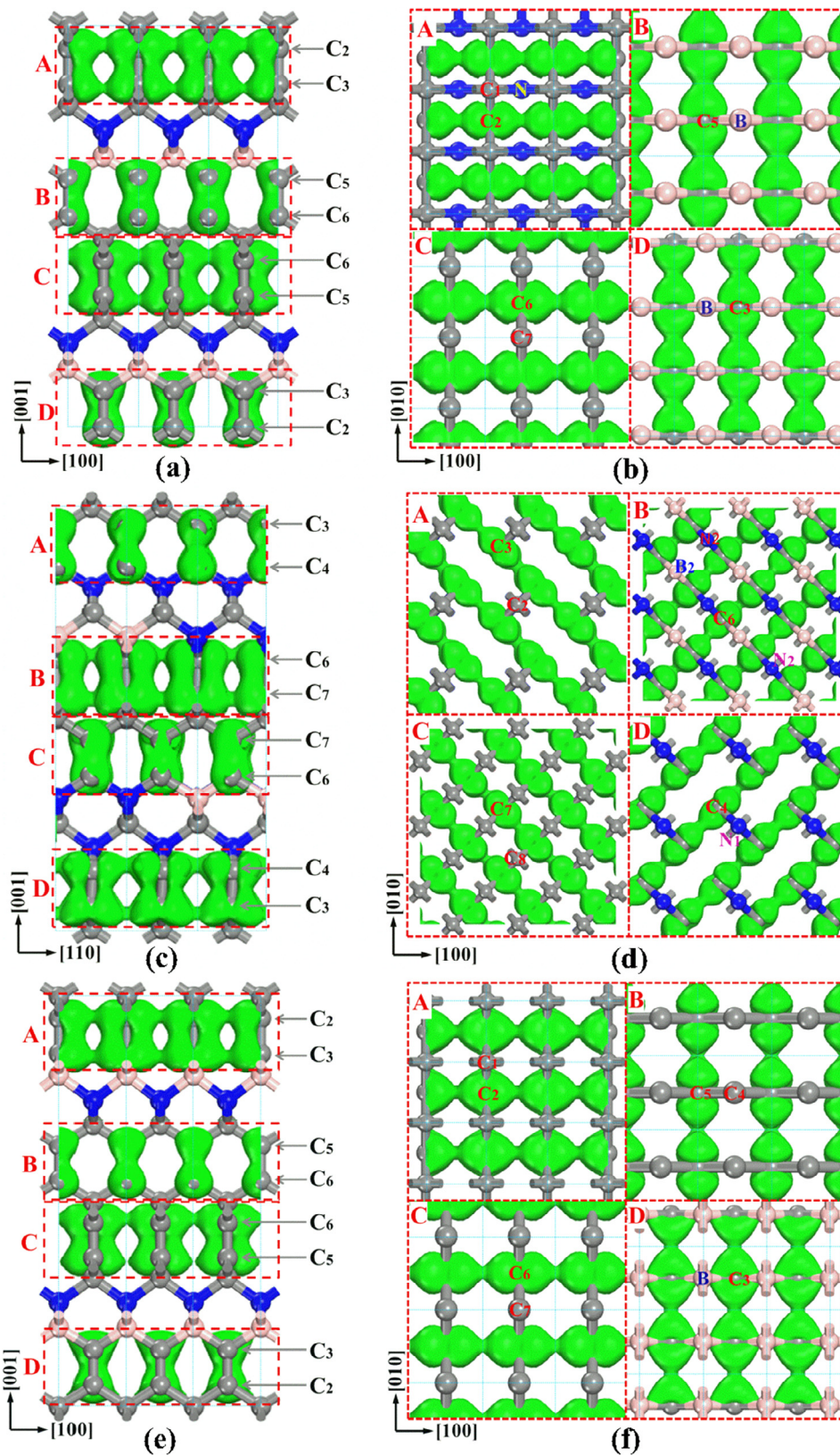


**Fig. 5.** Calculated electron orbits of *o*-BC<sub>6</sub>N, *t*-BC<sub>6</sub>N-1, and *t*-BC<sub>6</sub>N-2 structures. Every electron orbit figure includes two electron orbit projections of electron orbit: the left projections are along the [0 1 0] direction in the *o*-BC<sub>6</sub>N and *t*-BC<sub>6</sub>N-1 structures and along the [1  $\bar{1}$  0] direction in the *t*-BC<sub>6</sub>N-2 structure; on the other hand, the right projections are corresponding projections in four regions, marked as A, B, C, and D in the left figures, along the [0 0 1] direction in the *o*-BC<sub>6</sub>N, *t*-BC<sub>6</sub>N-1, and *t*-BC<sub>6</sub>N-2 structures, respectively.

**Table 3**  
Chemical bond parameters and Vickers hardness of *o*-BC<sub>6</sub>N.

Bond type	<i>d</i>	Pop	<i>P<sub>c</sub></i>	<i>N<sub>e</sub></i>	<i>f<sub>i</sub></i>	<i>f<sub>m</sub></i> (10 <sup>-3</sup> )	<i>H<sub>v</sub></i>
C1–C2	1.522	0.87	0.87	0.628	0	0.779	52.4
C2–C3	1.344	1.44	1.47	1.042	0.057	1.136	
C3–C4	1.505	0.94	0.90	0.650	0.096	0.645	
C5–C6	1.359	1.44	1.47	1.009	0.057	1.486	
C6–C7	1.550	0.85	0.87	0.595	0.063	2.035	
C4–N1	1.607	0.62	0.80	0.515	0.363	0.363	
N1–B1	1.604	0.65	0.80	0.460	0.313	0.409	
C5–B1	1.555	0.93	0.90	0.526	0.079	2.868	

**Table 4**  
Chemical bond parameters and Vickers hardness of *t*-BC<sub>6</sub>N-1.

Bond type	<i>d</i>	Pop	<i>P<sub>c</sub></i>	<i>N<sub>e</sub></i>	<i>f<sub>i</sub></i>	<i>f<sub>m</sub></i> (10 <sup>-3</sup> )	<i>H<sub>v</sub></i>
C1–C2	1.538	0.87	0.87	0.609	0	0.280	45.3
C2–C3	1.362	1.43	1.47	1.003	0.071	0.483	
C4–C5	1.514	0.94	0.90	0.639	0.096	0.853	
C5–C6	1.347	1.43	1.47	1.037	0.071	1.360	
C6–C7	1.529	0.86	0.87	0.620	0.037	0.807	
B4–N1	1.612	0.64	0.80	0.454	0.329	0.612	
N1–C4	1.595	0.63	1.21	0.526	0.688	0.401	
C3–B1	1.548	0.93	0.90	0.079	0.079	3.389	

**Table 5**  
Chemical bond parameters and Vickers hardness of *t*-BC<sub>6</sub>N-2.

Bond type	<i>d</i>	Pop	<i>P<sub>c</sub></i>	<i>N<sub>e</sub></i>	<i>f<sub>i</sub></i>	<i>f<sub>m</sub></i> (10 <sup>-3</sup> )	<i>H<sub>v</sub></i>
C1–C3	1.56982	0.84	0.85	0.573	0.038	0.323	40.1
C2–C3	1.52057	0.83	0.85	0.631	0.064	0.323	
C3–C4	1.34099	1.47	1.45	1.051	0.042	0.552	
C6–C7	1.33848	1.48	1.45	1.057	0.038	0.342	
C7–C8	1.5593	0.84	0.85	0.585	0.038	0.342	
C4–B1	1.57622	0.89	0.88	0.505	0.036	0.360	
C5–B1	1.60589	0.81	0.78	0.401	0.087	1.493	
C5–B2	1.60941	0.81	0.78	0.399	0.087	1.501	
C6–B2	1.58114	0.89	0.88	0.501	0.036	0.370	
C4–N1	1.51975	0.69	0.88	0.699	0.351	0.288	
C5–N1	1.58892	0.6	0.78	0.553	0.370	1.149	
C5–N2	1.58451	0.61	0.78	0.537	0.353	0.134	
C6–N2	1.51423	0.69	0.88	0.707	0.351	0.295	

are shown in Table 3–5, respectively. In this study we obtained the pure covalent population *P<sub>c</sub>* by calculating the overlap population of the C–C bonds in 2 × 2 × 1 supercells based on the corresponding BC<sub>6</sub>N structures. The calculated Vickers hardness of *o*-BC<sub>6</sub>N, *t*-BC<sub>6</sub>N-1, and *t*-BC<sub>6</sub>N-2 are 52.4, 45.3, and 40.1 GPa, respectively, which indicates that they are the potential superhard materials.

#### 4. Conclusions

In this work, three novel *sp*<sup>2</sup>–*sp*<sup>3</sup> hybridized BC<sub>6</sub>N phases are predicted and investigated in detail using first-principle calculations. These sandwich-like structural BC<sub>6</sub>N are similarly constructed from interlinked C multi-layers blocks stacking with one BN block along the *c* axis. The structural stabilities of these phases have been confirmed using the calculations of elastic stiffness constants and phonon spectra. The band structures show that these phases may process a metallic character. The calculated results of DOS and PDOS suggest that the main contributions to the metallicity in the three structures come from the *p* orbitals of *sp*<sup>2</sup>-bonded C atoms. *Sp*<sup>3</sup>-hybridized B, C, and N atoms form the isolation strips with a role in blocking electronic conduction. In the *o*-BC<sub>6</sub>N and *t*-BC<sub>6</sub>N-1 structures, the electrons can transmit along the chains, consisting of parallel C<sub>2</sub>–C<sub>3</sub> and C<sub>5</sub>–C<sub>6</sub> diatomic units at the [1 0 0] or the [0 1 0] crystal directions in different layers. In the *t*-BC<sub>6</sub>N-2 structure, the electrons in different layers can transmit

along the parallel, distributing C<sub>3</sub>–C<sub>4</sub> and C<sub>6</sub>–C<sub>7</sub> diatomic chains at the [1̄ 1 0] crystal orientations and [1 1 0] crystal orientations. These results indicate that *o*-BC<sub>6</sub>N, *t*-BC<sub>6</sub>N-1 and *t*-BC<sub>6</sub>N-2 crystals possess an interesting 1D metallicity with the orthogonal directionality between the alternant atomic layers. Thus, these materials can be used for measuring field strength and direction. The calculated theoretical Vickers hardness of *o*-BC<sub>6</sub>N, *t*-BC<sub>6</sub>N-1 and *t*-BC<sub>6</sub>N-2 are 52.4, 45.3, and 40.1 GPa, respectively, which indicate the potential use as superhard conductive materials.

#### Acknowledgements

This work was supported by the National Science Foundation of China (Grants Nos. 51421091, 51332005, 51572235, and 51672238).

#### References

- [1] N.V. Novikov, Synthesis of superhard materials, *J. Mater. Process. Technol.* 161 (1–2) (2005) 169–172.
- [2] N. Dubrovinskaia et al., Aggregated diamond nanorods, the densest and least compressible form of carbon, *Appl. Phys. Lett.* 87 (8) (2005) 083106.
- [3] N. Dubrovinskaia et al., Superior wear resistance of aggregated diamond nanorods, *Nano Lett.* 6 (4) (2006) 824–826.
- [4] I. Caretti et al., Friction and wear of amorphous BC<sub>6</sub>N coatings under different atmospheres, *Diam. Relat. Mater.* 16 (4–7) (2007) 1445–1449.

- [5] L. Vel et al., Cubic boron nitride: synthesis, physicochemical properties and applications, *Mater. Sci. Eng. B* 10 (2) (1991) 149–164.
- [6] B.P. Singh, Characterization of cubic boron nitride compacts, *Mater. Res. Bull.* 21 (1) (1986) 85–92.
- [7] V.L. Solozhenko et al., Synthesis of superhard cubic BC<sub>2</sub>N, *Appl. Phys. Lett.* 78 (10) (2001) 1385–1387.
- [8] E. Knittle et al., High-pressure synthesis, characterization, and equation of state of cubic C-BN solid solutions, *Phys. Rev. B* 51 (18) (1995) 12149–12156.
- [9] Kawaguchi et al., Preparation and electronic state of graphite-like layered material BC<sub>6</sub>N, *Synth. Met.* 125 (2) (2001) 259–263.
- [10] X. Luo et al., Refined crystal structure and mechanical properties of superhard BC<sub>4</sub>N crystal: first-principles calculations, *J. Phys. Chem. C* 112 (25) (2008) 9516–9519.
- [11] H. Sun et al., Structural forms of cubic BC<sub>2</sub>N, *Phys. Rev. B* 64 (9) (2001) 094108.
- [12] X. Luo et al., First-principles study of wurtzite BC<sub>2</sub>N, *Phys. Rev. B* 76 (9) (2007) 092107.
- [13] X. Luo et al., Ground-state properties and hardness of high density BC<sub>6</sub>N phases originating from diamond structure, *J. Appl. Phys.* 101 (8) (2007) 083505.
- [14] X. Luo et al., Prediction of graphitelike BC<sub>4</sub>N from first-principles calculations, *J. Appl. Phys.* 105 (4) (2009) 043509.
- [15] M. Mattesini, S.F. Matar, Search for ultra-hard materials: theoretical characterisation of novel orthorhombic BC<sub>2</sub>N crystals, *Int. J. Inorg. Mater.* 3 (7) (2001) 943–957.
- [16] Y. Zhang et al., Superhard cubic BC<sub>2</sub>N compared to diamond, *Phys. Rev. Lett.* 93 (19) (2004) 195504.
- [17] Q. Hu et al., Thermal oxidation behavior of hexagonal BC<sub>2</sub>N, *Mater. Charact.* 60 (1) (2009) 56–59.
- [18] A.R. Badzian, Cubic boron nitride - diamond mixed crystals, *Mater. Res. Bull.* 16 (11) (1981) 1385–1393.
- [19] J.L. He et al., First-principles study of B<sub>2</sub>CN crystals deduced from the diamond structure, *J. Phys.: Condens. Matter* 16 (46) (2004) 8131–8138.
- [20] Y. Li et al., High-energy density and superhard nitrogen-rich B-N compounds, *Phys. Rev. Lett.* 115 (10) (2015) 105502.
- [21] Y. Gao et al., Superhard sp<sup>2</sup>-sp<sup>3</sup> hybridized BC<sub>2</sub>N: a 3D crystal with 1D and 2D alternate metallicity, *J. Appl. Phys.* 121 (22) (2017) 225103.
- [22] M.D. Segall et al., First-principles simulation: ideas, illustrations and the CASTEP code, *J. Phys.: Condens. Matter* 14 (11) (2002) 2717–2744.
- [23] Y. Wang et al., CALYPSO: a method for crystal structure prediction, *Comput. Phys. Commun.* 183 (10) (2012) 2063–2070.
- [24] J. Lv et al., Predicted novel high-pressure phases of lithium, *Phys. Rev. Lett.* 106 (1) (2011) 015503.
- [25] Y. Wang et al., Crystal structure prediction via particle swarm optimization, *Physics* 82 (9) (2010) 7174–7182.
- [26] L. Zhu et al., Reactions of xenon with iron and nickel are predicted in the Earth's inner core, *Sci. Found. China* 6 (7) (2014) 644–648.
- [27] J.P. Perdew et al., Generalized gradient approximation made simple, *Phys. Rev. Lett.* 77 (18) (1996) 3865.
- [28] D. Vanderbilt, Soft self-consistent pseudopotentials in a generalized eigenvalue formalism, *Phys. Rev. B: Condens. Matter* 41 (11) (1990) 7892.
- [29] H.J. Monkhorst, J.D. Pack, Special points for Brillouin-zone integrations, *Phys. Rev. B* 13 (12) (1976) 5188–5192.
- [30] S. Baroni et al., Green's-function approach to linear response in solids, *Phys. Rev. Lett.* 58 (18) (1987) 1861.
- [31] Fischer et al., General methods for geometry and wave function optimization, *J. Phys. Chem.* 96 (24) (1992) 9768–9774.
- [32] F. Gao et al., Hardness of covalent crystals, *Phys. Rev. Lett.* 91 (1) (2003) 015502.
- [33] J. He et al., Ionicities of boron-boron bonds in B(12) icosahedra, *Phys. Rev. Lett.* 94 (1) (2005) 015504.
- [34] X. Guo et al., Hardness of covalent compounds: roles of metallic component and d valence electrons, *J. Appl. Phys.* 104 (2) (2008) 023503.
- [35] M. Ma et al., A metallic superhard boron carbide: first-principles calculations, *PCCP* 17 (15) (2015) 9748–9751.
- [36] M. Mattesini et al., First-principles characterisation of new ternary heterodiamond BC<sub>2</sub>N phases, *Comput. Mater. Sci.* 20 (1) (2001) 107–119.
- [37] Y. Tateyama et al., Proposed synthesis path for heterodiamond BC<sub>2</sub>N, *Phys. Rev. B* 55 (55) (1997) 10161–10164.
- [38] Y. Zhang et al., Influence of carbon content on the strength of cubicBC<sub>x</sub>N: a first-principles study, *Phys. Rev. B* 77 (9) (2008) 094120.
- [39] J.P. Watt, Hashin-Shtrikman bounds on the effective elastic moduli of polycrystals with orthorhombic symmetry, *J. Appl. Phys.* 50 (10) (1979) 6290–6295.